Determination of the plutonium content and O/M ratio of (U,Pu)O2-x using Raman spectroscopy

L. Medyk, D. Manara, J.-Y. Colle, D. Bouexière, J.F. Vigier, Loic Marchetti, Patrick Simon, Ph. Martin

Journal of Nuclear Materials 541 (2020) 152439

Contents lists available at ScienceDirect

Journal of Nuclear Materials

journal homepage: www.elsevier.com/locate/jnucmat

Determination of the plutonium content and O/M ratio of $(U,Pu)O_{2-x}$ using Raman spectroscopy

L. Medyk[a], D. Manara[b,c,*], J.-Y. Colle[c], D. Bouexière[c], J.F. Vigier[c], L. Marchetti[a], P. Simon[d], P.h. Martin[a]

[a] CEA, DES, ISEC, DMRC, Marcoule, Université de Montpellier, Bagnols sur Cèze, France
[b] European Commission, Joint Research Centre (JRC), Ispra, Italy
[c] European Commission, Joint Research Centre (JRC), Karlsruhe, Germany
[d] CNRS UPR 3079 CEMHTI, Université Orléans, 45071 Orléans, France

ARTICLE INFO

Article history:
Received 13 June 2020
Revised 22 July 2020
Accepted 30 July 2020
Available online 7 August 2020

Keywords:
Nuclear safety
Raman spectroscopy
Oxygen stoichiometry
Nuclear fuel characterization
$(U,Pu)O_{2-x}$

ABSTRACT

Oxygen stoichiometry in $(U,Pu)O_{2-x}$ nuclear fuels, while of prime interest, is still difficult to be determined at the micrometric scale. It has been recently evidenced that Raman microscopy is a promising tool to characterize $(U,Pu)O_{2-x}$ samples at a microscopic scale by probing the oxygen sublattice. Its use for determining the local O/M ratio was studied in this work on mixed oxide samples mostly containing ^{239}Pu and natural uranium, in addition to minor traces of other isotopes, including decay products and ^{241}Am. The first step was to dissociate the influence of the Pu/(U+Pu+Am) content, self-irradiation and O/M ratio on Raman spectra and especially on the main Raman band position in fluorite structure, the T_{2g}. In this aim, freshly annealed and aged $U_{1-y}Pu_yO_{2-x}$ samples, with $0.19 < y < 0.46$ and different O/M ratios, were analyzed by XRD and Raman spectroscopy. After figuring out that self-irradiation alone had no significant impact on the T_{2g} position, two mathematical relations were determined, linking the T_{2g} position to the Pu/(U+Pu+Am) content and to the lattice parameter. Finally, the oxygen hypostoichiometry direct impact on $(U,Pu)O_{2-x}$ Raman spectra was determined for the first time. In agreement with past results observed in CeO_{2-x}, a O/M ratio decrease induces a T_{2g} shift towards lower frequencies in $(U,Pu)O_{2-x}$. Combining the whole results, an equation allowing to determine the T_{2g} position according to the O/M ratio and Pu/(U+Pu+Am) content was established. Raman spectrometer associated to a confocal optical microscope can then be used to determine locally (≈1 μm) either the Pu/(U+Pu+Am) content or the O/M ratio. This study proves the relevance of such method to characterize the fuel pellets in an industrial way.

1. Introduction

Uranium-plutonium mixed dioxide, $U_{1-y}Pu_yO_{2-x}$, is currently studied for its future use as fuel for the next generation nuclear Sodium-cooled Fast Reactors (Na-FNR). Compared to the $(U,Pu)O_2$ fuels presently used in light water reactors, which are composed with about 7 mol.% Pu/(U+Pu), the Pu/(U+Pu) content range for fast reactor applications is planned to be significantly higher, within 20 and 40 mol.%. Moreover, to avoid cladding corrosion during irradiation, the Na-FNR fuel has to be oxygen hypostoichiometric, thus its Oxygen/Metal ratio (O/M with M=U+Pu) is typically lower than 2.00. Because the O/M ratio significantly affects most of the fuel properties (thermal conductivity, melting temperature, diffusion phenomena, fuel/cladding interactions, *etc.*) [1], its accurate determination is mandatory. Furthermore, considering that a small decrease of the O/M ratio induces a variation of the thermal conductivity which triggers a local temperature increase in the fuel under irradiation [2], the homogeneity of the O/M ratio at the grain scale across the fuel pellet is of prime interest. While the global oxygen stoichiometry in $(U,Pu)O_2$ of a fuel pellet can be determined by thermogravimetry, X-Ray Diffraction (XRD) [3,4] or X-ray Absorption Spectroscopy (XAS) [5–10], the O/M ratio variation remains extremely challenging to be investigated at the grain scale (≈ 5–10 μm).

Talip et al. [11,12] and Elorrieta et al. [13] evidenced that Raman microscopy is a promising tool for probing the oxygen sublattice of $(U,Pu)O_2$ fluorite materials. All along the 0–100% Pu/(U+Pu)

* Corresponding author at: European Commission, Joint Research Centre (JRC), Ispra, Italy.
E-mail address: dario.manara@ec.europa.eu (D. Manara).

https://doi.org/10.1016/j.jnucmat.2020.152439

content range, the $(U,Pu)O_{2.00}$ system can be considered as a Pu-doping of UO_2 where Pu^{4+} ions replace progressively the U^{4+} ions. An ideal solid solution, which conserves the fluorite structure [14], is formed and the lattice parameter decreases following a Vegard's law [15]. In Raman spectroscopy, the fluorite structure, included in the $Fm\bar{3}m$ symmetry group, is characterized by one first-order Raman mode, belonging to the T_{2g} irreducible representation, and a second-order mode, the 2 (T_{1u}LO) [16]. The T_{2g} mode corresponds to a symmetric stretching of the oxygen network. In $(U,Pu)O_{2.00}$ spectra, its position varies from 445 cm^{-1} for $UO_{2.00}$ [17–20] to around 478 cm^{-1} for $PuO_{2.00}$ [17,21–23]. A shift towards higher frequencies [13,24] of the T_{2g} band is then observed with the Pu/(U+Pu) content increase [13,24]. The 2 (T_{1u}LO) is the first overtone of the LO counterpart of the T_{1u} mode, which corresponds to asymmetric stretching of the O-M bands.

In the U–Pu–O phase diagram, a stability domain of a single $(U,Pu)O_{2\pm x}$ fluorite phase exists along a large range of x [14]. At room temperature, within the $U_{1-y}Pu_yO_{2+x}$ domain from y = 0.15 to 1 and up to x = 0.33, the lattice accepts additional oxygen atoms located in interstitial positions. Preserving the electroneutrality, a fraction of U^{4+} is oxidized to U^{5+} ions which leads, for a given Pu/(U+Pu) content, to a lattice parameter decrease [25,26]. In the hypostoichiometric $U_{1-y}Pu_yO_{2-x}$ domain, present up to $x > 0.02$ for $y > 0.2$, a fraction of the Pu^{4+} is reduced to Pu^{3+}, then oxygen vacancies are created and the lattice parameter increases [27]. Any variation of the O/M ratio induces therefore structural changes which trigger a local lattice distortion in the $(U,Pu)O_{2\pm x}$ phase. Hyperstoichiometry effects on $(U,Pu)O_{2+x}$ Raman spectra were studied by Elorrieta et al. [13]. The lattice parameter decrease, induced by the hyperstoichiometry (O/M < 2.25), led to a high-frequency T_{2g} band shift while the local disorder increase triggered a T_{2g} band broadening and the activation of two new Raman modes. The first at ~575 cm^{-1}, corresponding to the T_{1u}LO mode, and the second at ~650 cm^{-1}. The latter band is also observed in U_4O_9 Raman spectra at ~630 cm^{-1} and it was associated to cuboctahedral type oxygen cluster defects by Desgranges et al. [20].. However, no Raman data are available for an accurate characterization of hypostoichiometric $(U,Pu)O_{2-x}$ samples, which is, as mentioned earlier, driver fuel for Generation Four sodium fast reactors. Nevertheless, $CeO_{2.00}$ reduction data obtained by Raman spectroscopy [28] can be used as a first-approach reference. CeO_2 is actually often considered as a structural surrogate of PuO_2 as both crystallize in the same fluorite structure and both materials can be oxygen hypostoichiometric. Associated with the oxygen vacancy formation and the partial reduction of Ce^{4+} to Ce^{3+} ions, a T_{2g} band shift towards lower frequencies was observed. Moreover, studying hypostoichiometric $(U,Ce)O_{2-x}$ samples, Elorrieta et al. [29] highlighted the activation of a new band at ~535 cm^{-1}, in addition of the T_{1u}LO mode, whose intensity increased with the Ce^{3+} concentration. Moreover, this band totally disappeared when the samples were oxidized. To complete, Epifano et al. [10] investigated $(U,Am)O_{2-x}$ solid solutions and observed Raman bands at ~535 cm^{-1}, ~575 cm^{-1} and at ~632 cm^{-1} while Am^{3+} and U^{4+}/U^{5+} were present in the material. This triplet band, at 535, 575 and 635 cm^{-1}, is also observed for (self)-irradiated UO_2 and PuO_2 samples [30–34] and commonly called the U1, U2 and U3 defect bands. Indeed, irradiation induces point defects, such as anion and cation Frenkel pairs, and triggers a lattice expansion [35,36]. A thermal treatment at minimum 1000 °C is needed to anneal these defects [37]. By comparing Raman spectra of a self-irradiated and an annealed $(U,Pu)O_2$ sample, Talip et al. [11,12] observed that the accumulation of defects due to the alpha decay impacts the Raman spectra similarly to the oxygen hyperstoichiometry: the T_{1u}LO (or U2) band intensity increases, the U1 and U3 bands are observed and the 2(T_{1u}LO) band intensity decreases. Moreover, a T_{2g} band broadening and a 2 cm^{-1} low-frequency shift are observed. For PuO_2 sample, the T_{2g} broadening was also highlighted and Villa et al. suggested that the T_{2g} band width could be directly used to quantify the sample ageing [32].

To summarize, Pu/(U+Pu) content, O/M ratio and self-irradiation have an impact on Raman spectra of $(U,Pu)O_{2-x}$ with T_{2g} band shift and broadening, and the appearance of new bands associated to defects. While the study on CeO_{2-x} shows that the oxygen hypostoichiometry has a significant impact on the T_{2g} position, the influence of the O/M ratio on $(U,Pu)O_2$ has still to be investigated before attempting to quantify it using Raman spectroscopy. As Raman data on $(U,Pu)O_2$ materials remains rare, the individual contribution of all these defect sources are not yet established and quantified.

The aim of this work is to investigate $(U,Pu)O_{2-x}$ microstructure variations to dissociate the different consequences of ^{239}Pu self-irradiation, hypostoichiometry and Pu/(U+Pu) content on the T_{2g} Raman band and to evaluate the possibility to locally determine the O/M value using Raman spectroscopy in samples containing ^{239}Pu and natural uranium. Thus, an original Raman spectroscopy study on $U_{1-y}Pu_yO_{2-x}$ samples, with $0.19 < y < 0.46$, is presented. Raman and XRD measurements were performed on self-irradiated and annealed samples at different O/M ratios in order to quantify the lattice parameter variation impact on the T_{2g} band position. For the first time, the oxygen hypostoichiometry impact on $(U,Pu)O_{2-x}$ Raman spectra was investigated. Two mathematical relations were derived linking the T_{2g} position to the lattice parameter and to the Pu/(U+Pu) content for all stoichiometric samples, allowing a local O/M ratio determination using Raman spectroscopy.

2. Experimental

2.1. Materials

The starting samples were $U_{1-y}Pu_yO_{2-x}$ fragments extracted from sintered pellets, averaging 1–5 mm^2 in surface area, with five Pu/(U+Pu) contents ranging from y = 0.19 up to 0.46. All the samples were manufactured by powder metallurgy process in the 90′s (for more manufacturing details see corresponding references in Table 1). The 0.19, 0.24, 0.35 and 0.46 contents were provided by CEA (Commissariat à l'Energie Atomique, Cadarache, France) and the 0.40 content was provided by JRC-Karlsruhe (Joint Research Centre, Germany). Furthermore, the 0.24 and 0.40 contents were both composed of two samples, called A and B, initially treated to obtain two different O/M ratios (O/M ≈ 2.00 and O/M ≈ 1.98). In total, seven different chemical compositions were studied. For all samples, the Pu isotopy were mainly composed of ^{239}Pu. The ^{238}Pu content was below 0.3 mol.% of the total Pu, therefore its irradiation effects can be reasonably neglected. Around 0.1 mol % of ^{241}Am was detected by EPMA, only due to beta decay of ^{241}Pu traces initially present in the sample. The formation of ^{241}Am was taken into account and the updated Pu content at the time of the measurements are given in Table 1.

Since their fabrication, thermal treatments at minimum 1230 °C, either in Ar or Ar/H_2, had been applied on the samples. These heat treatments removed self-irradiation defects and possibly modified also the initial O/M ratio [35]. The time elapsed between the last annealing treatment and the reported measurements, so the self-irradiation defect accumulation time, is mentioned in Table 1.

In order to anneal self-irradiation defects accumulated since the last annealing and obtain a O/M ratio close to 2.00, a subsequent thermal treatment was performed on a fragment of the MOX19; MOX23.6-B; MOX34.7; MOX39.4-B; MOX45.6 samples. Pellet fragments were heated under Ar/6% H_2 + 1500 vpm H_2O atmosphere at 1450 °C during 20 h.

Table 1
Details of starting samples. Notation 1) corresponds to the sintering and 2) to the heat treatment performed to adjust the O/M ratio.

Sample name	Pu/(U+Pu+Am) (mol.%)	Sintering process at the manufacturing	O/M ratio at manufacturing	Time between last annealing and experiment (y)	Reference
MOX19	19.0	Ar/5% H_2 + 90 ppm H_2O, 1750 °C / 4 h	1.98	3	[38]
MOX23.6-A	23.6	–	1.978	3	[39]
MOX23.6-B	23.6	–	2.00	3	[39]
MOX34.7	34.7	1) Ar/5% H_2 +2300 ppm H_2O, 1700 °C / 24 h 2) Ar/5%H_2, 1500 °C	1.922	4.5	[40,41]
MOX39.4-A	39.4	1) Ar/1%H_2 1650 °C / 6 h 2) Ar/5%H_2, 1350 °C / 12 h	1.971	2.8	[42]
MOX39.4-B	39.4	Ar 1650 °C / 6 h	1.995	2.8	[42]
MOX45.6	45.6	1) Ar/5% H_2 +2300 ppm H_2O, 1700 °C / 24 h 2) Ar/5% H_2, 1500 °C	1.912	4.5	[40,41]

XRD and EPMA analyses performed after fabrication on MOX23.6-A and MOX23.6-B samples revealed that they were composed of approximately 10 vol% of UO_2 agglomerates, the average size of which is approximately 10 µm, and 90% of $U_{0.765}Pu_{0.235}O_2$ matrix. Small Pu-rich agglomerates of about 1 µm were also observed [39].

In this paper, the annealed samples will be called annealed-MOX and the as-self-irradiated samples aged-MOX.

2.2. Raman spectroscopy

Raman measurements were performed with a Jobin-Yvon T64000 Horiba equipped with a diode laser (λ=532 nm) and a Kr^+ laser (λ=647.5 nm). The laser beams were focused on the sample through a long focal distance (1 cm) objective (Numerical Aperture = 0.5) with 50x magnification. The laser spot size on the sample was of the order of 1 μm^2. The excitation power was optimized to prevent as much as possible any risk of sample oxidation by the beam: 12–15 mW (λ=532 nm) and 6–10 mW (λ=647.5 nm) measured at the objective exit using a power meter. Due to their high radiotoxicity, the samples were encapsulated into a dedicated sample holder designed by JRC- Karlsruhe [43]. The Raman measurements were performed through a 2-mm thick quartz window on top of the capsule resulting in an actual power at the sample surface of 2–3 mW for the laser with λ=532 nm and 1–2 mW for λ=647.5 nm [43]. The scattered radiation was filtered by an edge filter in order to remove the Rayleigh light, then dispersed using a 1800 grooves/mm holographic grating and recorded by a liquid-nitrogen cooled CCD detector.

The spectrometer was daily calibrated measuring a Raman spectrum of monocrystalline Si and adjusting the spectrometer position so the T_{2g} band was set at 520.5 cm^{-1}. The absolute instrumental uncertainty was estimated to be ± 1 cm^{-1}, whereas the repeatability upon comparing successive measurements is at least twice better. To prevent any spectral artefact due to sample porosity and/or local chemical inhomogeneity, a minimum of 3 spectra were collected at different locations for each sample. For all the biphasic MOX-23.6 samples, composed with 10% of UO_2 agglomerates, only the spectra corresponding to the (U,Pu)O_2 matrix were selected. The spectra of pure UO_2, recognizable by the strongly enhanced 2 (T_{1u}LO) band [16] when using green laser, were not taken into account.

Data acquisition was carried out with the LabSpec® 5 software (Horiba) and spectral treatment was performed with the LabSpec® 6.4 software. After subtraction of the baseline modeled using a fourth to eighth degree polynomial function, Raman bands were fitted using a function including Gaussian and Lorentzian contributions. From these fits, the position, width and intensity of each band can be obtained.

2.3. XRD

XRD analyses were performed with a Bruker D8-Advance diffractometer installed in a glove box dedicated for radioactive sample handling. A Cu X-ray source was used and Cu Kα2 radiation was removed thanks to a Germanium monochromator. The diffractometer was set in the Bragg-Brentano $\theta/2\theta$ geometry. About 20 mg of each sample were grinded into a fine powder for the XRD analyses. The diffractograms were recorded from $15° < 2\theta < 120°$ each 0.02° Rietveld refinements were performed with the Jana 2006 software [44].

2.4. Uncertainty determination

All the uncertainties given in the paper are expanded uncertainties and are given for a confidence level of 95%. Moreover, all the uncertainties given for calculated values were estimated by considering the Gaussian error propagation from the uncertainties on experimental measurements.

3. Results

3.1. XRD results

The $U_{1-y}Pu_yO_{2-x}$ samples, aged and annealed, were analyzed by XRD in order to determine their lattice parameter. For the aged samples, the lattice parameter values were corrected from self-irradiation swelling using the relation determined by Kato et al. [35]. From these raw (for annealed samples) or corrected (for aged samples) values, the O/M ratio was calculated using the relation determined by Duriez et al. (Eq. (1)) validated for $0 < y < 0.46$ [3,45].

$$a = 5,470 - 0,074\,y + 0,32\,x \quad (1)$$

with a (Å) the lattice parameter, y the Pu molar fraction and x the difference to the oxygen stoichiometry.

All these results are gathered in Table 2. All the annealed samples as well as aged-MOX34.7, aged-MOX39.4-A and aged-MOX45.6 samples display a lattice parameter close to the one corresponding to oxygen stoichiometry, with an O/M ratio > 1.99. The aged-MOX23.6-A, aged-MOX23.6-B and aged-MOX39.4-B samples were hypostoichiometric with O/M ratio < 1.99. According to Thermo-Calc [46] simulation, with a Pu/(U+Pu+Am) content of 39.4 mol.% and a O/M ratio equal to 1.976, aged-MOX39.4-B sample should be within the miscibility gap domain and then biphasic. However, two experimental investigations [40,47] showed that these conditions correspond to the miscibility gap boarder and considering the uncertainty, our result can be considered as accurate.

As previous analyses showed, the MOX23.6-A and MOX23.6-B samples were biphasic, composed of a majority phase of (U,Pu)O_2 and about 10% of a minor phase whose lattice parameter was close to UO_2 agglomerates.

Table 2
Lattice parameters (Å) and T_{2g} band positions of $(U,Pu)O_2$ samples, aged and annealed.

	Pu/(U+Pu+Am) (mol.%)	Average T_{2g} position (cm^{-1}) (from 3 to 26 measurements)	Raw lattice parameter (± 1.10^{-3} Å)	Corrected lattice parameter (± 1.10^{-3} Å) [35]	O/M *via* Eq. (1) ± 4.10^{-3}
Annealed samples	19	452.8 ± 0.4	5.458		1.993
	23.6 - B	454.6 ± 0.6	Biphasic: 90% = 5.453 10% = 5.469		1.999
	34.7	459.0 ± 1.0	5.446		1.996
	39.4 - B	460.5 ± 0.5	5.443		1.993
	45.6	462.7 ± 1.0	5.439		1.991
Aged samples	19	449.3 ± 0.8	Technical problem: not available		
	23.6 - A	452.8 ± 1.2	Biphasic: 85% = 5.464 15% = 5.472	Matrix 85%: 5.457	1.988
	23.6 - B	452.5 ± 5.4	Biphasic: 91% = 5.465 9% = 5.476	Matrix 91%: 5.458	1.983
	34.7	457.5 ± 2.0	5.457	5.447	1.993
	39.4 - A	460.5 ± 2.0	5.450	5.442	1.996
	39.4 - B	458.6 ± 2.3	5.456	5.448	1.976
	45.6	462.4 ± 1.3	5.451	5.439	1.991

3.2. Raman

3.2.1. Annealed samples

The first Raman measurements were performed on the annealed samples to investigate the Pu/(U+Pu+Am) content effect on the spectra separated from any other varying parameter (Fig. 1). The main band between 445 and 465 cm^{-1} corresponds to the T_{2g} mode. Its position,[1] determined by deconvolution as represented in Fig. 1b and given in Table 2 shifts towards high frequencies according to the Pu/(U+Pu+Am) content. The same trend was already evidenced in the literature [13,24]. A weaker band is visible around 580 cm^{-1}. It can be associated to the T_{1u} LO band which is activated by the disorder (structural and/or chemical) in the fluorite-type structure. In this case, as all the samples were close to the oxygen stoichiometry, a probable source of disorder would be the radius difference between U^{4+} and Pu^{4+} (1.001 Å [18] and 0.96 Å [48] respectively). The 2 (T_{1u}LO), corresponding to the second order of the T_{1u}LO band, is present at ~1150 cm^{-1} [49,50] for the lowest Pu/(U+Pu+Am) contents, 19 mol.% and 23.6 mol.%. The disappearance of this band with the Pu/(U+Pu+Am) content increase was already evidenced in previous studies [13]. An additional band, not yet assigned, is present around 900 cm^{-1}, at a wavelength close to the hypothetical second harmonic of the T_{2g} line. This band partially overlaps a broad bump between 950 cm^{-1} and 1050 cm^{-1}, a spectral range where Villa - Aleman et al. identified the Pu's Γ_1-Γ_4 crystal electric field transition [23]. Without further experiment, it remains however not possible to clearly attribute this band.

3.2.2. Aged samples

In Fig. 2, Raman spectra of the aged samples are represented. After at least 2.8 years of storage in inert atmosphere, structural defects due to self-irradiation accumulated in the samples [51]. Their presence created an expansion of the lattice parameter and enhanced the structural disorder: compared to Fig. 1, the T_{2g} band widened and the LO band intensity increased [12,36].

The T_{2g} band positions and FWHM obtained by deconvolution with the approach represented in Fig. 2b are summarized in Table 2 and Table 3, respectively. In the latter, the accumulation of alpha decay damage is taken into account by calculating the alpha self-irradiation dose $\lambda' t$, where λ' is alpha decay constant and t is the self-irradiation time as described in [35].

[1] The expanded uncertainties associated to the average T_{2g} positions given in Table 2 were all estimated using the Student's *t*-distribution for a confidence level of 95% (see Section 2.4). They can thus vary significantly from one sample to another depending on the number of measurements made on each sample.

4. Discussion

In order to dissociate the different effects of the self-irradiation, the hypostoichiometry and the Pu/(U+Pu+Am) content on Raman spectra, and especially on the T_{2g} band position, aged and annealed $U_{1-y}Pu_yO_{2-x}$ samples (with $0.19 < y < 0.456$) were studied. The annealing procedure largely removed self-irradiation damages and set the O/M ratio close to 2.00, as shown by XRD analyses (Table 2). Indeed, all the annealed samples exhibited an O/M ratio higher than 1.99. This value was taken as the low limit above which the samples, from this work or from the literature [13,24], can be considered as "stoichiometric".

Regarding the differences observed between aged and annealed samples, the intensity band variations of the 2(T_{1u}LO) and T_{1u}LO are obvious. However, a quantitative comparison would be thorny. Indeed, the high intensity of the 2(T_{1u}LO) band is linked to a resonance effect [16], which depends on the electronic density of states of the material. The closer is the laser energy to an electronic transition gap, the more enhanced appears the band intensity. Unfortunately, the electronic property variations into $(U,Pu)O_2$ samples as a function of O/M ratio and Pu/(U+Pu+Am) content are not known yet. The present discussion is then focused mostly on the T_{2g} band position and width.

4.1. Annealed samples

To dissociate the Pu/(U+Pu+Am) content effect from those of the self-irradiation and the hypostoichiometry, the annealed samples were first studied separately. In

Fig. 3, the T_{2g} positions determined for annealed samples (given in Table 2), are plotted vs. the Pu/(U+Pu+Am) content (a) and the lattice parameter (b), and compared to the values available in the literature [13,24]. In order to achieve a numerical fit as accurate as possible, only samples close to the oxygen stoichiometry (O/M > 1.99) extracted from studies giving sufficient information (lattice parameter and/or O/M ratio) were considered. Therefore, only the data from Böhler et al.'s study were taken into account in the present analysis and the 9 mol.%, 40 mol.% and 50 mol.% Pu/(U+Pu+Am) points were left out as their O/M ratio was lower than 1.99.

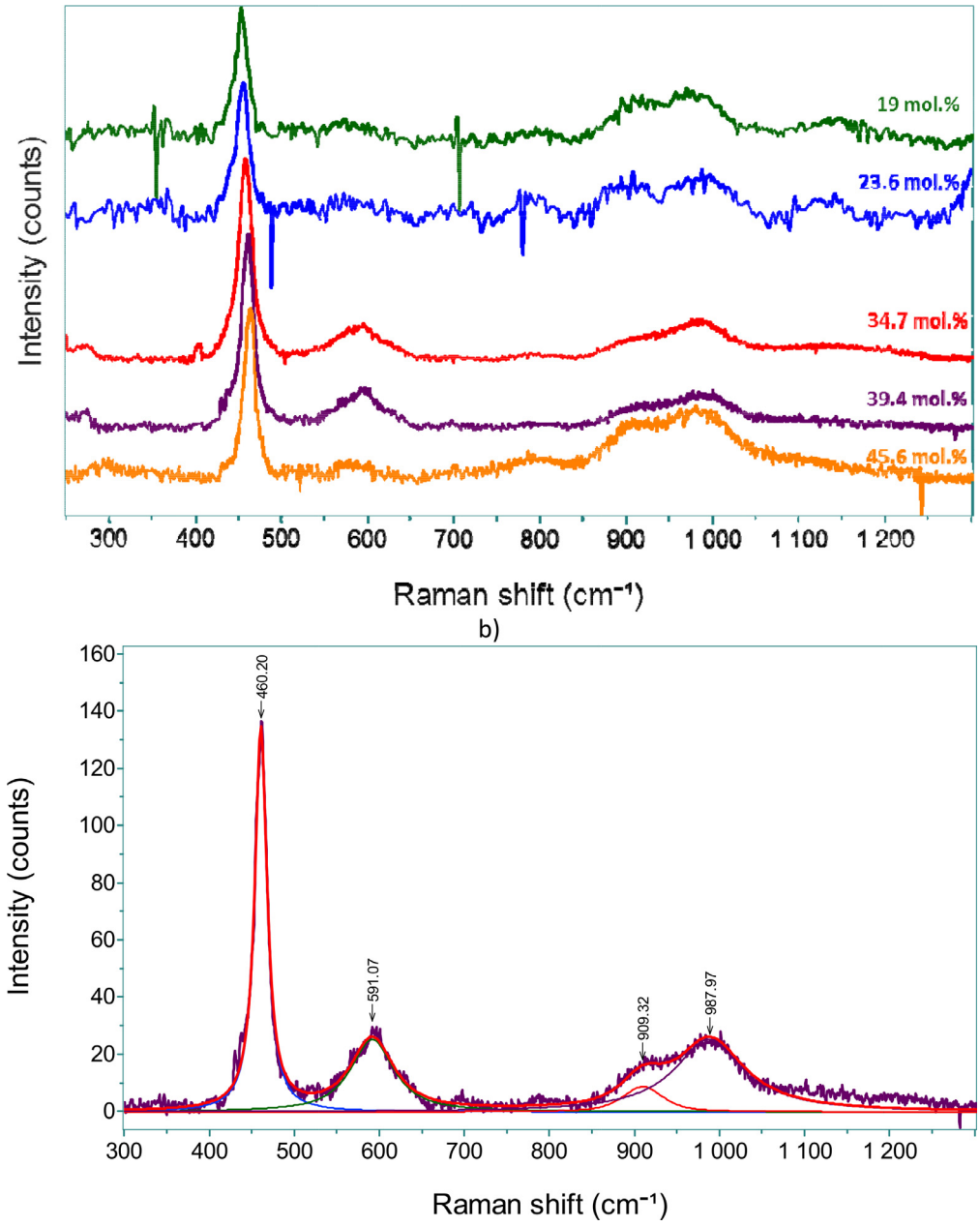

Fig. 1. a) Raman spectra of annealed and stoichiometric $(U,Pu)O_{2.00}$ samples; laser wavelength: 532 nm. b) Example of deconvolution method with the annealed-MOX39.4 spectrum.
The negative spikes are artefacts due to a defective CCD pixel.

Table 3
Average T_{2g} widths and width increases due to self-irradiation. The * corresponds to the aged hypostoichiometric samples. $\lambda' t$ is the alpha self-irradiation dose, where λ' is alpha decay constant and t the self-irradiation time as described in [35].

Sample	Accumulated alpha defect $\lambda' t$	Average T_{2g} width (cm^{-1}) – aged samples	Average T_{2g} width (cm^{-1}) – annealed samples	Width increase (%) due to self-irradiation
MOX19	3.08×10^{-5}	31.0	17.4	43.9
MOX23.6 - A	5.09×10^{-5}	26.1*	20.4	20.5*
MOX23.6 - B	5.09×10^{-5}	28.15*		27.3*
MOX34.7	8.11×10^{-5}	27.4	17.9	34.6
MOX39.4 - A	6.07×10^{-5}	29.8	19.1	36.0
MOX39.4 - B	6.07×10^{-5}	22.3*		14.5*
MOX45.6	1.07×10^{-4}	22.4	16.3	27.3

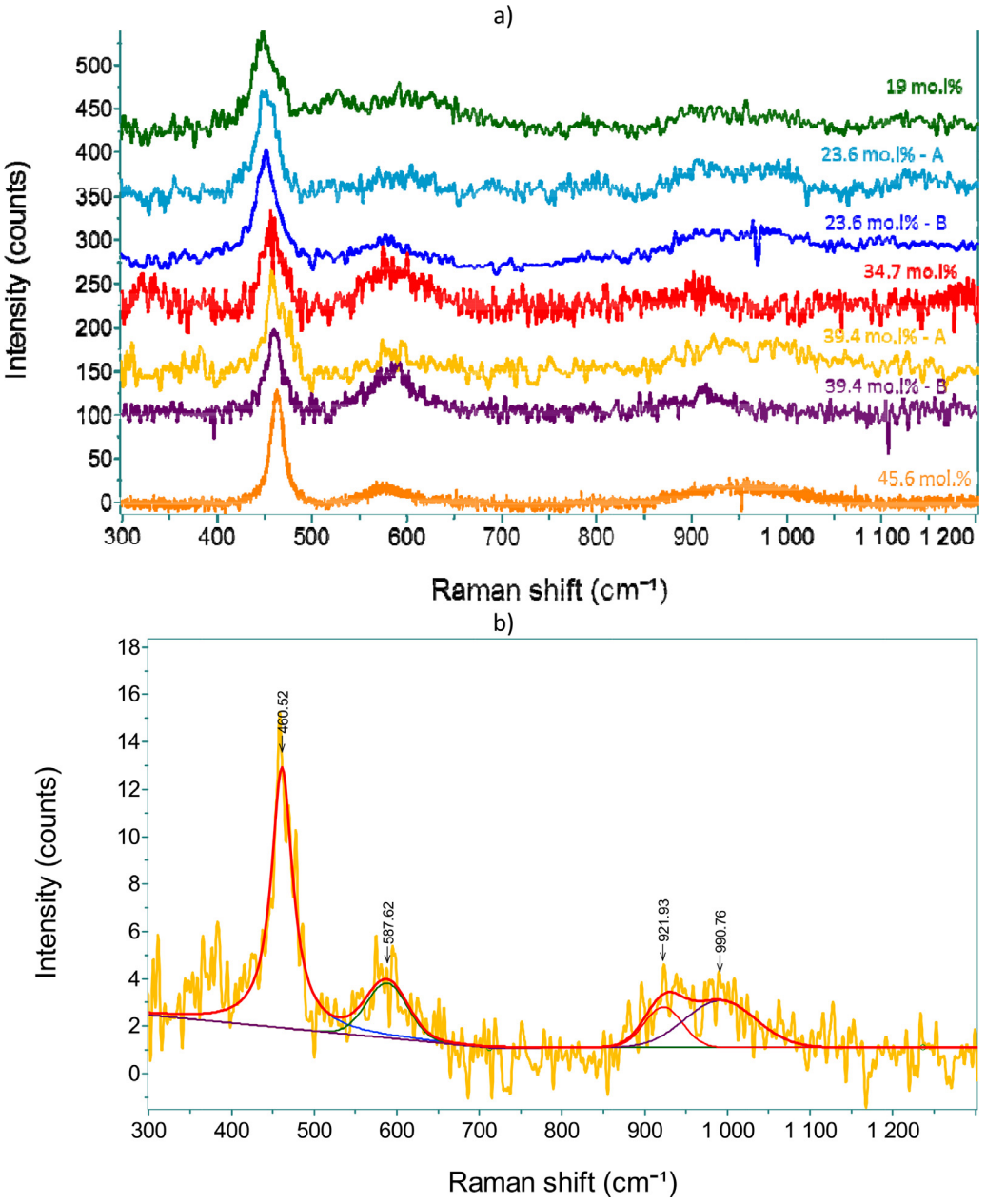

Fig. 2. a) Raman spectra of aged $(U,Pu)O_{2-x}$ samples. All spectra were obtained using the 532-nm laser except the aged-MOX34.7 (red) and aged-MOX39.4-B (purple) spectra which were obtained using the 660-nm laser. b) Deconvolution example with aged-MOX39.4-A spectrum.
The negative spikes are artefacts due to a defective CCD pixel. (For interpretation of the references to color in this figure legend, the reader is referred to the web version of this article.)

The T_{2g} band position plots can be fitted with a second degree polynomial function. However, according to the software used, the coefficients deduced from the fitting of experimental data were not exactly identical, which probably reveals some convergence issues during the fitting routine. While the plots of the Pu/(U+Pu+Am) content and the lattice parameter as a function of the T_{2g} position can be fitted by square root functions, Eq. (2) and Eq. (3) respectively, whose coefficients are identical regardless of the software used to perform fitting. Therefore, the equations of the polynomial functions plotted in

Fig. 3a and b, Eq. (4) and Eq. (5), were not determined from a direct fitting routine but derived from Eq. (2) and Eq. (3) respectively.

$$\%Pu = k_1 \times \sqrt{k_2 - \omega} + k_3 \quad (2)$$

$$a = h_1 \times \sqrt{h_2 - \omega} + h_3 \quad (3)$$

$$\omega = \mathrm{A} \times \%Pu^2 + \mathrm{B} \times \%Pu + \mathrm{C} \quad (4)$$

$$\omega = \mathrm{A}' \times a^2 + \mathrm{B}' \times a + C' \quad (5)$$

with *%Pu* (mol.%) the Pu/(U+Pu+Am) content (for stoichiometric samples), a (Å) the lattice parameter, ω (cm^{-1}) the T_{2g} band position and:

$k_1 = (-28.2 \pm 1.0)cm^{1/2}$ $k_2 = (485.7 \pm 1.9)cm^{-1}$
$k_3 = (180.0 \pm 8.4)$
$h_1 = (1.861 \pm 0.040) \times 10^{-2} cm^{1/2}.Å$ $h_2 = (482.1 \pm 1.0)cm^{-1}$
$h_3 = (5.3569 \pm 0.0024)Å$

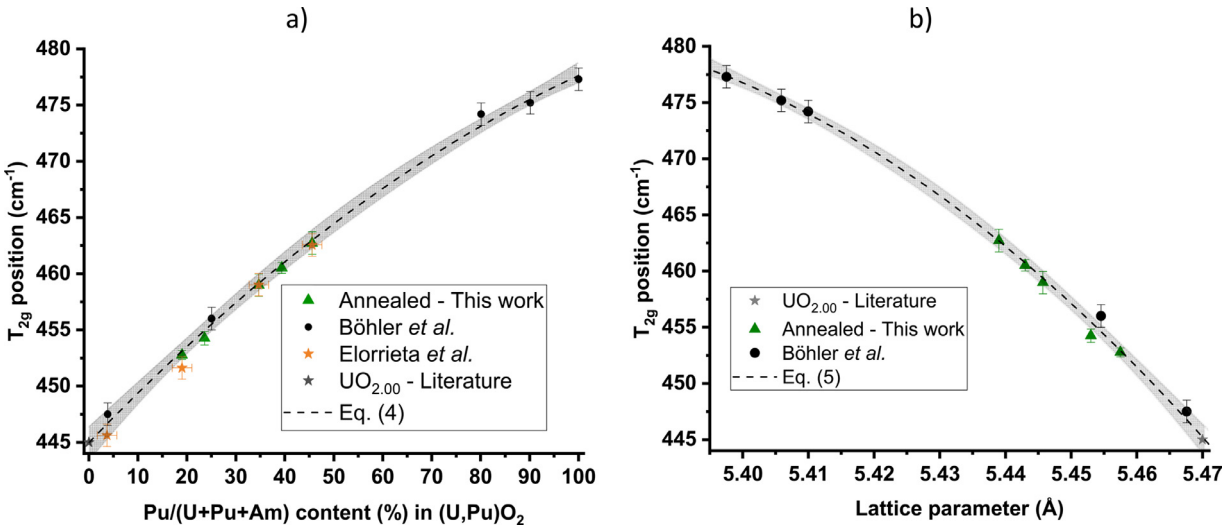

Fig. 3. T_{2g} position of $(U,Pu)O_{2.00}$ samples as a function of a) the Pu/(U+Pu+Am) content (mol.%) and b) the lattice parameter (Å) – Combination with literature data from Böhler et al. [24] (black dots) and for UO_2 [2,3,21–24] (grey stars) to perform fitting (dashed line) (see text for details). The grey bands represent the expanded uncertainty on T_{2g} position derived from Eq. (4) and Eq. (5) with a confidence level of 95%. Comparison with Elorrieta et al. [13] (orange stars).(For interpretation of the references to color in this figure legend, the reader is referred to the web version of this article.)

$$A' = -2.890 \times 10^3 cm^{-1}.Å^{-2} \quad B' = 3.090 \times 10^4 cm^{-1}.Å^{-1}$$
$$C' = -8.240 \times 10^4 cm^{-1}$$

$$A = -1.256 \times 10^{-3} cm^{-1} \quad B = 4.521 \times 10^{-1} cm^{-1}$$
$$C = 4.450 \times 10^2 cm^{-1}$$

The data obtained by Elorrieta et al. [13] on stoichiometric samples were not taken into account in our fit calculations as no lattice parameter was provided in the paper, hindering the exact determination of the O/M ratios. However, their experimental points are in good agreement with Eq. (4) determined for annealed and stoichiometric samples.

Moreover, using Vegard's law Eq. (1) with x=0) applied to the $(U,Pu)O_{2,00}$ system, an equation linking the T_{2g} position to the Pu/(U+Pu+Am) content can be deduced from Eqs. (1) and ((3):

$$\omega = h_2 - \left(\frac{5.47 - 0.00074 \times \%Pu - h_3}{h_1}\right)^2 \quad (6)$$

with %Pu (mol.%) the Pu/(U+Pu+Am) content and h_1 = (1.861 ± 0.040).10^{-2} $cm^{1/2}$.Å; h_2 = (482.1 ± 1.0) cm^{-1}; h_3 = (5.3569 ± 0.0024) Å

The results are plotted in Fig. 4 (red curve). The T_{2g} position according to the Pu/(U+Pu+Am) for O/M = 2.00 (Eq. (4)) is also plotted (black line). Along the whole Pu/(U+Pu+Am) range, the difference between T_{2g} positions given by the two curves is never greater than 1 cm^{-1}, so equal to the instrumental uncertainty. Hence, the hypothesis of considering as stoichiometric all samples exhibiting an O/M ratio > 1.99 can be considered as accurate.

4.2. Aged samples

To investigate the influence of self-irradiation of ^{239}Pu and traces of ^{241}Am on the T_{2g} position, its values for the aged samples are plotted as a function of the Pu/(U+Pu+Am) content (Fig. 5a) and the lattice parameter (Fig. 5b) and compared with the polynomial fit obtained for the annealed samples.

The O/M ratios of the aged samples, given in Table 2, were obtained by using the cell parameter values corrected from self-irradiation swelling (detailed Section 3.1). The aged-MOX34.7, aged-MOX39.4-A and aged-MOX45.6 samples can be considered as stoichiometric with O/M > 1.99 whereas the remaining samples (aged-MOX23.6-A, aged-MOX23.6-B and aged-MOX39.4-B) are hypostoichiometric (O/M < 1.99). In

Fig. 5a, the samples are then split into two groups: the stoichiometric (full red squares) and the hypostoichiometric ones (empty red squares). The self-irradiation effect on the T_{2g} band position could be then evaluated comparing the stoichiometric aged samples with Eq. (4) linking the T_{2g} position and the Pu/(U+Pu+Am) content for stoichiometric and self-irradiation defect-free samples (black line). The T_{2g} band positions for these three aged samples match with Eq. (4). This shows that the self-irradiation defects have little or no impact on the T_{2g} position.

The same Fig. 5a displays also the oxygen hypostoichiometry effect on the T_{2g} position. This can be appreciated by comparing aged-MOX23.6-A, aged MOX23.6-B and MOX39.4-B (the open red squares on

Fig. 5a) with all the other points. Their T_{2g} band position was systematically shifted towards lower frequencies as the O/M ratio decreased.

These two conclusions - no self-irradiation impact on the T_{2g} band position and T_{2g} band shift towards lower frequencies because of the oxygen hypo-stoichiometry – are consistent with the plot in

Fig. 5b. In the latter, the T_{2g} band position of the aged samples is represented as a function of the raw lattice parameter (red squares) and the corrected one (blue points). For comparison, the polynomial function corresponding to the annealed samples (Eq. (5)) is also plotted in

Fig. 5b. The raw lattice parameter points are systematically above the polynomial function, without displaying any particular trend. On the other hand, the corrected lattice parameter points, independently from their O/M ratio, are situated on the plot of Eq. (5). This illustrates that, for a given Pu/(U+Pu+Am) content, the T_{2g} band position is not impacted, in the present samples, by the lattice expansion due to self-irradiation. Moreover, the hypostoichiometry effect can be apprehended considering the two 39.4 mol.% points, as the first is stoichiometric and the second corresponds to an O/M ratio of 1.976. These 2 points match Eq. (5), however in agreement with the lattice parameter increase due to the hypostoichiometry, the T_{2g} position of the second point (hypostoichiometric) is shifted towards lower frequencies.

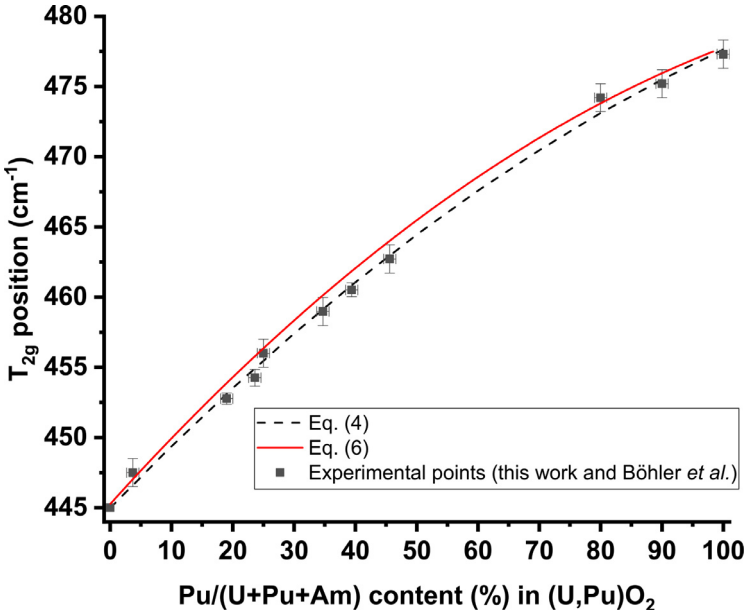

Fig. 4. Comparison between the curve of the T_{2g} position according to the Pu/(U+Pu+Am) content (mol.%) derived from stoichiometric samples data, with $1.991 < O/M < 1.999$, (Eq. (4), black line) and the theoretical curve for $O/M = 2.00$ derived from Eq. (6) (red line). The black dots correspond to the experimental points from this work and from Böhler et al.'s study [24]. (For interpretation of the references to color in this figure legend, the reader is referred to the web version of this article.)

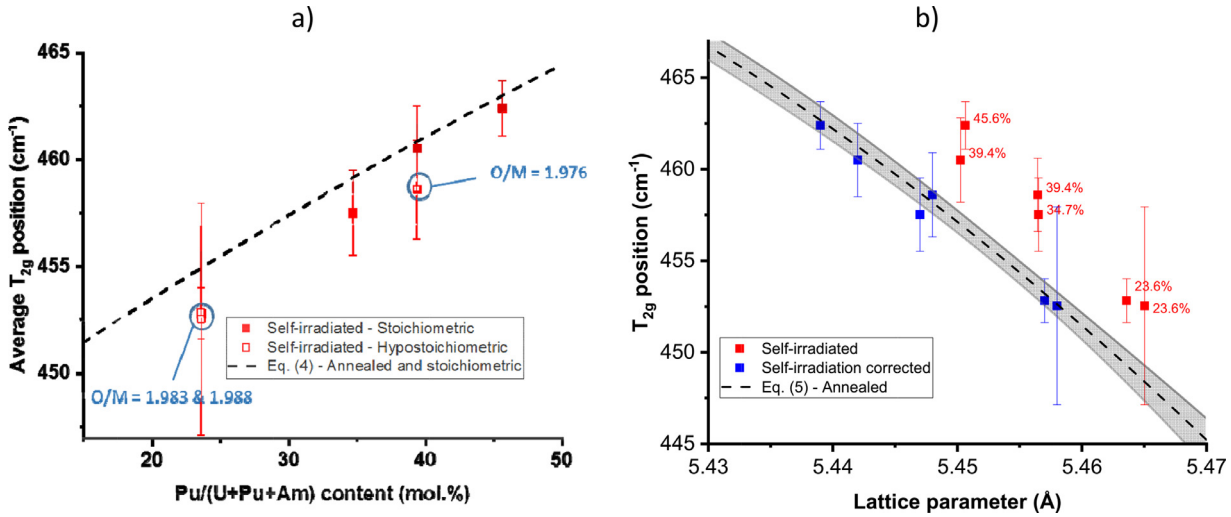

Fig. 5. T_{2g} position of $(U,Pu)O_{2-x}$ samples as a function of a) the Pu/(U+Pu+Am) content (mol.%) b) the lattice parameter (raw: red squares and corrected: blue pentagons) – polynomial functions determined for annealed sample points, Eq. (4) and Eq. (5), are represented as reference (black dash lines). The grey bands represent the expanded uncertainty on T_{2g} position derived from Eq. (4) and Eq. (5) with a confidence level of 95%. (For interpretation of the references to color in this figure legend, the reader is referred to the web version of this article.)

The results on the self-irradiation effect tend to disagree with those of Talip *et al*[11]., who assumed that the T_{2g} low-frequency shift observed on an aged sample was due to the lattice swelling. However, our results show that the Raman-active vibration frequencies of the oxygen cage are not modified by the accumulation of alpha self-irradiation defects. At a first sight, this observation can be puzzling. In fact, it can be explained by noticing that the self-irradiation effects are essentially studied here by XRD analysis on the cation sub-lattice, whereas Raman spectroscopy essentially detects anion sublattice vibrations, at least for wavenumbers larger than 200 cm^{-1}. The point defects created by alpha self-irradiation actually cluster and grow into dislocation loops that trigger the swelling. In this work, XRD is the main characterization tool used to observe and quantify the swelling, and intrinsically to this technique only the cation sublattice is probed. To the best of our knowledge, no experimental data is available on the oxygen sublattice being influenced by alpha self-irradiation of ^{239}Pu and traces of ^{241}Am. Furthermore, molecular dynamic simulation data [52] support the current interpretation, by showing that oxygen defects recover with a much higher rate than the cation sublattice. Thus, the mentioned facts can explain the current observation, that self-irradiation damage has no significant impact on the Raman-detected oxygen sublattice vibrations. One can then regard the present data as relevant experimental evidence of the separation between self-irradiation effects on the cation and the anion sub-lattices.

Concerning Talip et al.'s results, thanks to the effect separation performed in the present analysis, the low-frequency shift of the T_{2g} band can be more soundly attributed to oxygen hypostoichiometry rather than self-irradiation swelling.

Nevertheless, if self-irradiation have little impact on the T_{2g} band position, one can observe in Table 3 that the FWHM of the

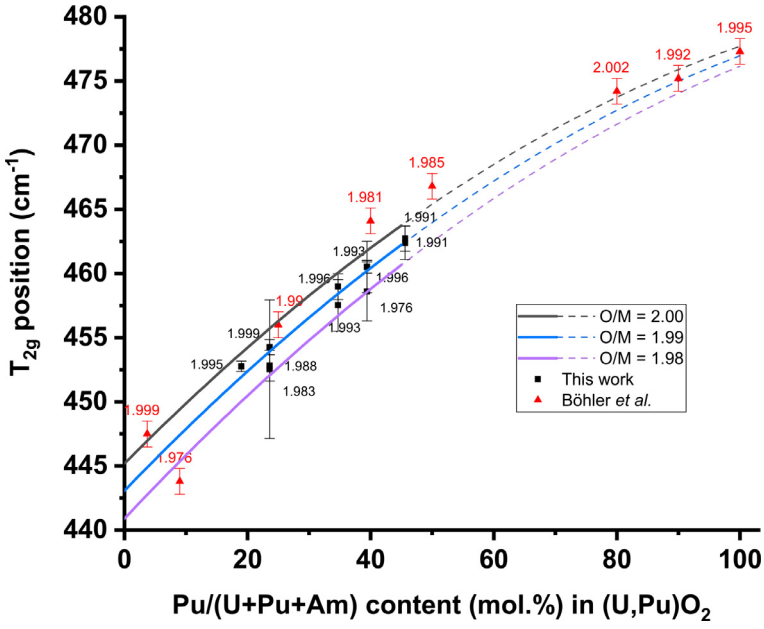

Fig. 6. Theoretical T_{2g} position curves obtained from Eq. (7) according to the Pu/(U+Pu+Am) content at different O/M ratios. The validity domain is represented with a solid line extended to 100% by a dashed line. The experimental points of this work (black squares) and from Böhler et al. (red triangles) are represented with their respective O/M ratio. (For interpretation of the references to color in this figure legend, the reader is referred to the web version of this article.)

T_{2g} band is larger in aged samples, as expected due to the disorder induced by self-irradiation and already evidenced by Villa-Aleman et al. [32]. This disorder affects mostly the cation sub-lattice. However, it is not obvious to predict the effects on the T_{2g} band features in oxygen hypo-stoichiometric samples, due to the combination between the self-irradiation disorder induced in the cation sub-lattice and the hypostoichiometry disorder induced in the anion sublattice. FWHM analysis performed in the present investigation by comparing self-irradiated and annealed, stoichiometric and hypostoichiometric samples yielded no obvious trend, and is therefore not reported here. Studying the behaviour of the same sample during a long timescale will help to clarify the Raman peak width behavior, which may be the object of further research.

In conclusion, Eq. (2) and Eq. (4), plotted in Fig. 3a, initially determined for annealed stoichiometric samples, can be considered now as valid for any stoichiometric sample, annealed or aged. And Eq. (3) allows determining the lattice parameter, corrected from self-irradiation defect for aged samples, from the T_{2g} band position. In addition, from the lattice parameter obtained, the O/M ratio can be determined when the Pu/(U+Pu+Am) content is known *via* Eq. (1).

Finally, combining Eq. (1) and Eq. (5), the cumulative curves of the T_{2g} position according to the Pu/(U+Pu+Am) content at different O/M ratios are derived in the following Eq. (7). The proposed relation Eq. (7) can be considered as valid in the 0–45 mol.% Pu/(U+Pu) range as it is based on Eq. (1) [45]. Nevertheless, this range can be extended to the whole Pu/(U+Pu+Am) content considering the relation Eq. (8) proposed by Kato et al. to determine the deviation from stoichiometry for $U_{1-z-y'-y''}Pu_zAm_{y'}Np_{y''}O_{2-x}$ samples [4].

$$\omega = \alpha + \beta \times \%Pu + \gamma \times x + \delta \times (\%Pu)^2 + \varepsilon \times x^2 + \zeta \times \%Pu \times x \quad (7)$$

with $\alpha = 4.452 \times 10^2$ cm^{-1} $\beta = 4.833 \times 10^{-1}$ cm^{-1} $\gamma = -2.090 \times 10^2$ cm^{-1} $\delta = -1.581 \times 10^{-3}$ cm^{-1} $\varepsilon = -2.957 \times 10^2$ cm^{-1} $\zeta = 1.367$ cm^{-1}

As a further step, the Am and Np contributions on the lattice parameter value should be also taken into account. However, due to the lack of information on the Am or Np contents and on the Am^{3+}/Am^{4+} ratio of our samples and from the literature, this relation could not be considered in this study.

$$a = \frac{4}{\sqrt{3}} \times [(r_U(1 - z - y' - y'') + r_{Pu}z + r_{Am}y' + r_{Np}y'') \times (1 + 0.112x) + r)_a] \quad (8)$$

with a (Å), the lattice parameter, r_U, r_{Pu}, r_{Am}, r_{Np} and r_a the ionic radius (Å) of respectively U^{4+}, Pu^{4+}, Am^{4+}, Np^{4+} and O^{2-}, x the deviation from stoichiometry.

In Fig. 6, the proposed curves obtained from Eq. (7) for O/M = 1.98; 1.99 and 2.00 are plotted. Our experimental points as well as those of Böhler et al.'s study are represented.

The present experimental points are consistent with the corresponding O/M curve except for aged-MOX34.7, whose calculated O/M ratios was 1.993 instead of 1.985 and. This discrepancy is most probably attributable to the uncertainty of the measurements. Böhler et al.'s points also well fit with the theoretical curves except for Pu/(U+Pu+Am) content 40mol% and 50 mol.%Pu/(U+Pu+Am). The T_{2g} positions observed are in disagreement with the cumulative curves as they are shifted of 5.3 cm^{-1} and 3.6 cm^{-1} towards higher frequencies. One explanation could be a sample oxidation between the time of XRD and Raman measurements.

5. Conclusion

This work was devoted to study separately the influence of the Pu/(U+Pu+Am) content, self-irradiation and O/M ratio on Raman spectra of $(U,Pu)O_{2-x}$ solid samples containing mostly ^{239}Pu and natural uranium, in addition to traces of ^{241}Am. The comparison between annealed and aged samples highlighted that the current self-irradiation had negligible impact on the T_{2g} position unlike it was assumed in previous literature [11, 12]. The shift observed by Talip et al. [11, 12] could be explained as being due to oxygen hypostoichiometry, rather than lattice swelling directly due to self-irradiation. One reasonable explanation of this unexpected result would be that the anion sublattice, probed by Raman microscopy, recover much quicker than the cation sublattice usually analysed by the conventional characterization tools. One can then regard the

present data as relevant experimental evidence of the separation between self-irradiation effects on the cation and the anion sublattices.

From this first conclusion, we were able to compare stoichiometric and hypostoichiometric samples and evidenced that the O/M ratio decrease triggered a T_{2g} band shift towards lower frequencies. The equations derived by fitting the current experimental points and some literature data permit to obtain the Pu/(U+Pu+Am) content or the lattice parameter at the micron scale starting from the T_{2g} Raman peak position. From the latter, the O/M ratio can also be obtained, as equation linking the T_{2g} position, the Pu/(U+Pu+Am) content and the deviation from the oxygen stoichiometry were also deduced.

It is thus shown that the Pu/(U+Pu+Am) content, the lattice parameter and consequently the O/M ratio are directly connected at the grain scale to vibrational bands easily detectable by Raman microscopy. Performing Raman cartographies, the variation of these fuel properties within a pellet can be imaged. Raman microscopy appears then to be a relevant tool to characterize fuel pellets, especially the local O/M ratio which was, up to now, challenging to be determined at the grain scale.

The present results can find useful applications in the effective microanalysis of nuclear fuel properties on a grain-size scale (1–10 µm). This is of great interest not only for the preparation of homogenous fuel elements for plants of the current and future generation, but also for the analysis and recycling of spent fuel and the study of segregation in elements extracted from severe accident sites.

Declaration of Competing Interest

The authors declare that they have no known competing financial interests or personal relationships that could have appeared to influence the work reported in this paper.

CRediT authorship contribution statement

L. Medyk: Investigation, Data curation, Formal analysis, Data curation, Visualization, Writing - original draft. **D. Manara:** Resources, Supervision, Validation, Writing - review & editing. **J.-Y. Colle:** Investigation, Validation, Data curation. **D. Bouexière:** Investigation. **J.F. Vigier:** Investigation, Validation, Data curation. **L. Marchetti:** Methodology, Writing - review & editing. **P. Simon:** Conceptualization, Supervision, Methodology, Writing - review & editing. **P.h. Martin:** Conceptualization, Supervision, Methodology, Project administration, Funding acquisition, Writing - review & editing.

Acknowledgments

This work has been partially supported by the ENEN+ project that has received funding from the EURATOM research and training Work Programme 2016 – 2017 – 1 #755576.

The present research is part of the projects ESNII+ and ESRF-SMART. The Authors are indebted to prof. R.J.M. Konings (JRC) for his advice.

Supplementary materials

Supplementary material associated with this article can be found, in the online version, at doi:10.1016/j.jnucmat.2020.152439.

References

[1] C. Guéneau, A. Chartier, L. Van Brutzel, 2.02 - thermodynamic and thermophysical properties of the actinide oxides, in: R.J.M. Konings (Ed.), Comprehensive Nuclear Materials, Elsevier, Oxford, 2012, pp. 21–59. http://www.sciencedirect.com/science/article/pii/B9780080560335000094 .

[2] M. Kato, K. Maeda, T. Ozawa, M. Kashimura, Y. Kihara, Physical properties and irradiation behavior analysis of Np- and Am-bearing MOX fuels, J. Nucl. Sci. Technol. 48 (2011) 646–653, doi:10.1080/18811248.2011.9711745.

[3] C. Duriez, J.-P. Alessandri, T. Gervais, Y. Philipponneau, Thermal conductivity of hypostoichiometric low Pu content $(U,Pu)O_{2-x}$ mixed oxide, J. Nucl. Mater. 277 (2000) 143–158, doi:10.1016/S0022-3115(99)00205-6.

[4] M. Kato, K. Konashi, Lattice parameters of $(U, Pu, Am, Np)O_{2-x}$, J. Nucl. Mater. 385 (2009) 117–121, doi:10.1016/j.jnucmat.2008.09.037.

[5] R. Vauchy, R.C. Belin, A.-C. Robisson, F. Lebreton, L. Aufore, A.C. Scheinost, P.M. Martin, Actinide oxidation state and O/M ratio in hypostoichiometric uranium–plutonium–americium $U_{0.750}Pu_{0.246}Am_{0.004}O_{2-x}$ mixed oxides, Inorg. Chem. 55 (2016) 2123–2132, doi:10.1021/acs.inorgchem.5b02533.

[6] D. Prieur, L. Martel, J.-F. Vigier, A.C. Scheinost, K.O. Kvashnina, J. Somers, P.M. Martin, Aliovalent cation substitution in UO2: electronic and local structures of U1–yLayO2±x solid solutions, Inorg. Chem. 57 (2018) 1535–1544, doi:10.1021/acs.inorgchem.7b02839.

[7] D. Prieur, P.M. Martin, A. Jankowiak, E. Gavilan, A.C. Scheinost, N. Herlet, P. Dehaudt, P. Blanchart, Local structure and charge distribution in mixed uranium–americium oxides: effects of oxygen potential and am content, Inorg. Chem. 50 (2011) 12437–12445, doi:10.1021/ic200910f.

[8] R.C. Belin, P.M. Martin, J. Lechelle, M. Reynaud, A.C. Scheinost, Role of cation interactions in the reduction process in plutonium–americium mixed oxides, Inorg. Chem. 52 (2013) 2966–2972, doi:10.1021/ic3023776.

[9] U. Carvajal-Nunez, D. Prieur, T. Vitova, J. Somers, Charge distribution and local structure of americium-bearing thorium oxide solid solutions, Inorg. Chem. 51 (2012) 11762–11768, doi:10.1021/ic301709d.

[10] E. Epifano, M. Naji, D. Manara, A.C. Scheinost, C. Hennig, J. Lechelle, R.J.M. Konings, C. Guéneau, D. Prieur, T. Vitova, K. Dardenne, J. Rothe, P.M. Martin, Extreme multi-valence states in mixed actinide oxides, Commun. Chem. 2 (2019) 1–11, doi:10.1038/s42004-019-0161-0.

[11] Z. Talip, S. Peuget, M. Magnin, L. Berardo, C. Valot, R. Vauchy, C. Jégou, Raman microspectroscopic studies of unirradiated homogeneous $(U_{0.76}Pu_{0.24})O_{2+x}$: the effects of Pu content, non-stoichiometry, self-radiation damage and secondary phases, J. Raman Spectrosc. 48 (2017) 765–772, doi:10.1002/jrs.5092.

[12] Z. Talip, S. Peuget, M. Magnin, M. Tribet, C. Valot, R. Vauchy, C. Jégou, Characterization of un-irradiated MIMAS MOX fuel by Raman spectroscopy and EPMA, J. Nucl. Mater. 499 (2018) 88–97, doi:10.1016/j.jnucmat.2017.11.014.

[13] J.M. Elorrieta, D. Manara, L.J. Bonales, J.F. Vigier, O. Dieste, M. Naji, R.C. Belin, V.G. Baonza, R.J.M. Konings, J. Cobos, Raman study of the oxidation in $(U, Pu)O_2$ as a function of Pu content, J. Nucl. Mater. 495 (2017) 484–491, doi:10.1016/j.jnucmat.2017.08.043.

[14] C. Sari, U. Benedict, H. Blank, A study of the ternary system UO-PuO-Pu_2O_3, J. Nucl. Mater. 35 (1970) 267–277.

[15] P. Buisson, Role de la distribution des compositions cationiques sur l'aptitude a la dissolution des combustibles mox caracterisation de la distribution par diffraction des rayons x sur poudre, Grenoble 1 (1999) http://www.theses.fr/1999GRE10159.

[16] T. Livneh, E. Sterer, Effect of pressure on the resonant multiphonon Raman scattering in UO_2, Phys. Rev. B 73 (2006) 085118, doi:10.1103/PhysRevB.73.085118.

[17] G.M. Begun, R.G. Haire, W.R. Wilmarth, J.R. Peterson, Raman spectra of some actinide dioxides and of EuF_2, J. Common Met. 162 (1990) 129–133, doi:10.1016/0022-5088(90)90465-V.

[18] Z. Talip, T. Wiss, P.E. Raison, J. Paillier, D. Manara, J. Somers, R.J.M. Konings, Raman and x-ray studies of uranium–lanthanum-mixed oxides before and after air oxidation, J. Am. Ceram. Soc. 98 (2015) 2278–2285, doi:10.1111/jace.13559.

[19] P. Marlow, J. Russell, J. Hardy, Raman scattering in uranium dioxide, Philos. Mag. 14 (1966) 409, doi:10.1080/14786436608219022.

[20] L. Desgranges, G. Baldinozzi, P. Simon, G. Guimbretière, A. Canizares, Raman spectrum of U_4O_9: a new interpretation of damage lines in UO_2, J. Raman Spectrosc 43 (2012) 455–458, doi:10.1002/jrs.3054.

[21] M.J. Sarsfield, R.J. Taylor, C. Puxley, H.M. Steele, Raman spectroscopy of plutonium dioxide and related materials, J. Nucl. Mater. 427 (2012) 333–342, doi:10.1016/j.jnucmat.2012.04.034.

[22] M. Naji, N. Magnani, L.J. Bonales, S. Mastromarino, J.-Y. Colle, J. Cobos, D. Manara, Raman spectrum of plutonium dioxide: vibrational and crystal field modes, Phys. Rev. B 95 (2017) 104307, doi:10.1103/PhysRevB.95.104307.

[23] E. Villa-Aleman, N.J. Bridges, T.C. Shehee, A.L. Houk, Raman microspectroscopy of PuO_2 particulate aggregates, J. Nucl. Mater. 515 (2019) 140–149, doi:10.1016/j.jnucmat.2018.12.022.

[24] R. Böhler, M.J. Welland, D. Prieur, P. Cakir, T. Vitova, T. Pruessmann, I. Pidchenko, C. Hennig, C. Guéneau, R.J.M. Konings, D. Manara, Recent advances in the study of the UO_2–PuO_2 phase diagram at high temperatures, J. Nucl. Mater. 448 (2014) 330–339, doi:10.1016/j.jnucmat.2014.02.029.

[25] L. Lynds, W.A. Young, J.S. Mohl, G.G. Libowitz, X-Ray and density study of nonstoichiometry in uranium oxides - advances in chemistry (ACS Publications), Adv. Chem. (1963) 58–65 https://pubs.acs.org/doi/abs/10.1021/ba-1964-0039.ch005. accessed December 7, 2018.

[26] J.M. Elorrieta, L.J. Bonales, N. Rodríguez-Villagra, V.G. Baonza, J. Cobos, A detailed Raman and X-ray study of UO_{2+x} oxides and related structure transitions, Phys. Chem. Chem. Phys. 18 (2016) 28209–28216, doi:10.1039/C6CP03800J.

[27] E.R. Gardner, T.L. Markin, R.S. Street, The plutonium-oxygen phase diagram, J. Inorg. Nucl. Chem. 27 (1965) 541–551, doi:10.1016/0022-1902(65)80259-7.

[28] H. Li, P. Zhang, G. Li, J. Lu, Q. Wu, Y. Gu, Stress measurement for nonstoichio-

metric ceria films based on Raman spectroscopy, J. Alloys Compd. 682 (2016) 132–137, doi:10.1016/j.jallcom.2016.04.272.
[29] J.M. Elorrieta, L.J. Bonales, S. Fernández, N. Rodríguez-Villagra, L. Gutiérrez-Nebot, V.G. Baonza, J. Cobos, Pre- and post-oxidation Raman analysis of (U, Ce)O2 oxides, J. Nucl. Mater. (n.d.). 10.1016/j.jnucmat.2018.05.042.
[30] R. Mohun, L. Desgranges, J. Léchelle, P. Simon, G. Guimbretière, A. Canizarès, F. Duval, C. Jegou, M. Magnin, N. Clavier, N. Dacheux, C. Valot, R. Vauchy, Charged defects during alpha-irradiation of actinide oxides as revealed by Raman and luminescence spectroscopy, Nucl. Instrum. Methods Phys. Res. Sect. B Beam Interact. Mater. At. 374 (2016) 67–70, doi:10.1016/j.nimb.2015.08.003.
[31] R. Mohun, L. Desgranges, C. Jégou, B. Boizot, O. Cavani, A. Canizarès, F. Duval, C. He, P. Desgardin, M.-F. Barthe, P. Simon, Quantification of irradiation-induced defects in UO_2 using Raman and positron annihilation spectroscopies, Acta Mater 164 (2019) 512–519, doi:10.1016/j.actamat.2018.10.044.
[32] E. Villa-Aleman, A.L. Houk, N.J. Bridges, T.C. Shehee, Raman spectroscopy: A tool to investigate alpha decay damage in a PuO_2 crystal lattice and determining sample age since calcination, J. Raman Spectrosc. 50 (2019) 899–901, doi:10.1002/jrs.5591.
[33] L. Desgranges, G. Guimbretière, P. Simon, F. Duval, A. Canizares, R. Omnee, C. Jégou, R. Caraballo, Annealing of the defects observed by Raman spectroscopy in UO2 irradiated by 25MeV He2+ ions, Nucl. Instrum. Methods Phys. Res. Sect. B Beam Interact. Mater. At. 327 (2014) 74–77, doi:10.1016/j.nimb.2013.10.083.
[34] G. Guimbretière, L. Desgranges, A. Canizarès, G. Carlot, R. Caraballo, C. Jégou, F. Duval, N. Raimboux, M.R. Ammar, P. Simon, Determination of in-depth damaged profile by Raman line scan in a pre-cut He2+ irradiated UO2, Appl. Phys. Lett. 100 (2012) 251914, doi:10.1063/1.4729588.
[35] M. Kato, A. Komeno, H. Uno, H. Sugata, N. Nakae, K. Konashi, M. Kashimura, Self-radiation damage in plutonium and uranium mixed dioxide, J. Nucl. Mater. 393 (2009) 134–140, doi:10.1016/j.jnucmat.2009.05.020.
[36] M. Noe, J. Fuger, Self-radiation effects on the lattice parameter of $^{238}PuO_2$, Inorg. Nucl. Chem. Lett. 10 (1974) 7–19, doi:10.1016/0020-1650(74)80211-4.
[37] W.J. Weber, Alpha-irradiation damage in CeO_2, UO_2 and PuO_2, Radiat. Eff. 83 (1984) 145–156, doi:10.1080/00337578408215798.
[38] personnal communication, internal CEA report, (n.d.).
[39] L. Aufore, M.-A. Martinez, J.-J. Margueron, B. D'Hers, E. Belval-Haltier, I. Felines, J.-M. Untrau, Y. Marc, J.-C. Richaud, M. Reynaud, R. Belin, A.-C. Robisson, F. Houette, P.M. Martin, N. Chauvin, P. Raison, D. Bouexière, O. Dieste Blanco, B. Cremer, T. Wiss, E. Dahms, D. Staicu, Characterisations of MOX-Fresh1 Fuel, European commission, 2017.
[40] T. Truphémus, R.C. Belin, J.-C. Richaud, M. Reynaud, M.-A. Martinez, I. Félines, A. Arredondo, A. Miard, T. Dubois, F. Adenot, J. Rogez, Structural studies of the phase separation in the UO_2–PuO_2–Pu_2O_3 ternary system, J. Nucl. Mater. 432 (2013) 378–387, doi:10.1016/j.jnucmat.2012.07.034.
[41] M. Strach, D. Manara, R.C. Belin, J. Rogez, Melting behavior of mixed U–Pu oxides under oxidizing conditions, Nucl. Instrum. Methods Phys. Res. Sect. B Beam Interact. Mater. At. 374 (2016) 125–128, doi:10.1016/j.nimb.2016.01.032.
[42] J. Somers, J.-P. Glatz, D. Haas, D.H. Wegen, S. Fourcaudot, S. Fuchs, A. Stalios, D. Plancq, G. Mühling, Status of the TRABANT Irradiation Experiments, Global '99 , International Conference on Future Nuclear Systems, 1999.
[43] M. Naji, J.-Y. Colle, O. Beneš, M. Sierig, J. Rautio, P. Lajarge, D. Manara, An original approach for Raman spectroscopy analysis of radioactive materials and its application to americium-containing samples, J. Raman Spectrosc. 46 (2015) 750–756, doi:10.1002/jrs.4716.
[44] V. Petříček, M. Dušek, L. Palatinus, Crystallographic computing system JANA2006: general features, Z. Für Krist. - Cryst. Mater. 229 (2014) 345–352, doi:10.1515/zkri-2014-1737.
[45] R. Vauchy, A.-C. Robisson, R.C. Belin, P.M. Martin, A.C. Scheinost, F. Hodaj, Room-temperature oxidation of hypostoichiometric uranium–plutonium mixed oxides $U_{1-y}Pu_yO_{2-x}$ – A depth-selective approach, J. Nucl. Mater. 465 (2015) 349–357, doi:10.1016/j.jnucmat.2015.05.033.
[46] C. Guéneau, N. Dupin, B. Sundman, C. Martial, J.-C. Dumas, S. Gossé, S. Chatain, F.D. Bruycker, D. Manara, R.J.M. Konings, Thermodynamic modelling of advanced oxide and carbide nuclear fuels: description of the U–Pu–O–C systems, J. Nucl. Mater. 419 (2011) 145–167, doi:10.1016/j.jnucmat.2011.07.033.
[47] J.-F. Vigier, P.M. Martin, L. Martel, D. Prieur, A.C. Scheinost, J. Somers, Structural investigation of (U0.7Pu0.3)O2-x mixed oxides, Inorg. Chem. 54 (2015) 5358–5365, doi:10.1021/acs.inorgchem.5b00392.
[48] A. Nakamura, A defect-thermodynamic approach to PuO and CeO, J. Nucl. Mater. 201 (1993) 17–26, doi:10.1016/0022-3115(93)90155-R.
[49] G.C. Allen, I.S. Butler, N.A. Tuan, Characterisation of uranium oxides by micro-Raman spectroscopy, J. Nucl. Mater. 144 (1987) 17–19, doi:10.1016/0022-3115(87)90274-1.
[50] D. Manara, B. Renker, Raman spectra of stoichiometric and hyperstoichiometric uranium dioxide, J. Nucl. Mater. 321 (2003) 233–237, doi:10.1016/S0022-3115(03)00248-4.
[51] A. Nakamura, New defect-crystal-chemical approach to non-Vegardianity and complex defect structure of fluorite-based MO_2–$LnO_{1.5}$ solid solutions (M^{4+} = Ce, Th; Ln^{3+} = lanthanide): part ii: detailed local-structure and ionic-conductivity analysis, Solid State Ion 181 (2010) 1631–1653, doi:10.1016/j.ssi.2010.09.022.
[52] H. Balboa, L. Van Brutzel, A. Chartier, Y. Le Bouar, Damage characterization of (U,Pu)O2 under irradiation by molecular dynamics simulations, J. Nucl. Mater. 512 (2018) 440–449, doi:10.1016/j.jnucmat.2018.07.056.